High-Precision Robust Force Control of a Series Elastic Actuator

Sehoon Oh, *Member, IEEE*, and Kyoungchul Kong, *Member, IEEE*

***Abstract*—A series elastic actuator (SEA) is a promising actuation method in force control applications that intelligently interacts with environments. The SEA is characterized by a spring placed between a load and an actuator, which is an electric motor in most cases. Since the spring plays the role of a transducer between position (i.e., the spring deflection) and force, it is able to control the output force (torque) precisely by utilizing typical position control methods. However, the force control performance of the SEA is considered to have limitations due to its elasticity, and thus, to be inferior to rigid actuators in terms of bandwidth. This paper proposes that the force control performance of the SEA can be improved by exploiting the dynamic model of the SEA. To this end, the SEA is modeled and analyzed utilizing the two-mass dynamic model, which is a well-known and widely accepted model of the flexible system. The disturbance observer and feedforward controller are introduced as the model-based control algorithms for the SEA to achieve the high-precision force control. In addition to high-bandwidth force control, the proposed controller can address the robust stability and performance against model parameter variance and exogenous disturbances. For the analytic and quantitative assessment of the proposed force control system, the dynamic characteristics of an SEA under various control algorithms are analyzed, and the experimental results are provided for an actual SEA system in this paper.**

***Index Terms*—Actuator control, force/torque mode control, motion control, series elastic actuator, transparent actuation.**

I. Introduction

FORCE is a fundamental measure of how materials interact with each other. The ultimate goal of environment-interactive mechatronic systems (EIMSs) is the precision control of the interactive force. For example, the safety of robot arms physically coworking with human operators is examined based on the magnitude of the interactive force [1], and the human assistive robots are force-mode controlled for natural assistance [2]. The more closely mechatronic systems interact with environments, the more significantly the precise force control is emphasized.

The stability and performance analyses for precise force control have been investigated by many researchers [3]–[6], where the location of the sensor and the flexibility of the sensor have been discussed as the key factors to the stability. In a realistic setting, interaction dynamics (e.g., compliance or flexibility) take place between the actuation system and the environment. For example, the mechanical frames and gears of robotic joints introduce a flexibility between the actuator and the environment. In the viewpoint of controls, the flexible connection introduces either a collocated mode or a noncollocated mode depending on the location of a sensor. When the flexibility is positioned between an actuator and a sensor, the system has a noncollocated mode. On the other hand, when the flexibility is out of the actuator and sensor system, the system has a collocated mode.

Eppinger *et al.* [5] has shown that the feedback gains for the force control with a soft sensor are limited when the sensor is located in a noncollocated mode, and accordingly, the bandwidth of a force controller is limited. Newman *et al.* analyzed the stability of the EIMS with a flexible sensor treating the whole system as a *two-port* system [3]. Although the input–output relationship of the two-port system is somewhat complicated due to the flexibility of the sensor unit, it was shown that the phase restriction problem could be relived, in particular, in a high frequency range. Based on these research results, it should be noticed that the series elastic actuator (SEA) can suffer from these stability and bandwidth limitation problems due to its elasticity to measure force.

Calanca *et al.* investigated the role of compliance in force control as well [7]. They adopted a simple stability condition proposed by Whitney [8], which requires $Tk_pk_e < 1$ where T is the sampling period, k_p is the proportional control gain, and k_e is the environmental stiffness. Starting from this stability condition, various aspects of SEA force control have been researched in terms of the compliance of the motor side and a more complicated environment model. One of the most widely accepted examples is the proportional-derivative (PD) control of force with the positive feedback control of load-side acceleration, proposed by Pratt *et al.* [9]. Galanca *et al.* updated this control

Manuscript received January 14, 2016; revised August 5, 2016; accepted September 11, 2016. Date of publication September 29, 2016; date of current version February 14, 2017. Recommended by Technical Editor H.-R. Choi. This work was supported in part by DGIST MIRE-BraiN Program of the Ministry of Science, ICT and Future Planning (2016010046), in part by the National Research Foundation of Korea (NRF) funded by the Korean Ministry of Science, ICT and Future Planning of Korea (MSIP) under Grant NRF-2013R1A1A2063460, and in part by the Agency of Defense Development of Korea (ADD) under the contract ADD-14-02-03-01.

S. Oh is with the Department of Robotic Engineering, Daegu Gyeongbuk Institute of Science and Technology, Daegu 42988, Korea (e-mail: sehoon@dgist.ac.kr).

K. Kong is with the Department of Mechanical Engineering, Sogang University, Seoul 04107, Korea (e-mail: kckong@sogang.ac.kr).

Color versions of one or more of the figures in this paper are available online at http://ieeexplore.ieee.org.

Digital Object Identifier 10.1109/TMECH.2016.2614503

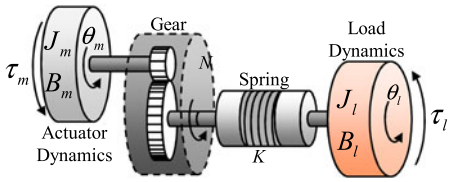

Fig. 1. Simplified models of SEAs.

law using a parameter adaptation algorithm [7]. Throughout the related studies, it has been proved that the flexibility or the compliance between the actuator and the environment provides various advantages and several limitations for achieving high-precision force control.

An SEA, which is shown in Fig. 1, imposes a precise flexibility on the EIMS; it utilizes an elastic transmission for transferring and measuring the actuation force. The elastic component converts the force control problem into a position control problem.

Many research groups have modeled SEA [10], [11] as one-mass model considering the load-side position deviation as external disturbance input. However, the dynamics of the SEA system can be modeled also as a two-mass system when the load-side dynamics is taken into account. By modeling an SEA as a two-mass system, the control of an SEA can benefit from conventional control algorithms designed for two-mass systems, which have long been studied in industrial applications [12], [13]. One thing to be noticed in this application of conventional control algorithms to the SEA is that the SEA focuses more on the control of the force transmitted through the elastic component, while the conventional two-mass systems pay more attention to the control of the load-side position.

It is true that there have been approaches to model an SEA as a two-mass system; for example, Boaventura *et al.* [14] utilized the two-mass system representation and proposed a force control method that utilizes the load-side velocity as the reference velocity for the motor side. Even though they utilized the two-mass model of an SEA, their control algorithm is not designed fully based on the dynamic model, and the model is utilized more for analysis.

This paper proposes a novel force controller for the SEA based on its dynamic model as a two-mass system. To this end, a disturbance observer (DOB) algorithm is applied to the spring deflection feedback control in this paper. The DOB makes the dynamic characteristics from the control input (i.e., the actuation force) to the spring deflection robust toward the external disturbance as well as the model variation of the load side, and therefore, the desired high-precision force control can be achieved based on the nominal model retained by the DOB. The proposed method is verified by: 1) interactive force (torque) tracking control and 2) the zero-impedance control (ZIC) experiments.

In spite of the significance of the SEAs as an identical force-mode actuation system in robotic applications, their dynamic characteristics have not yet been fully explored and analyzed for the design of controllers, in particular, the DOB. This paper provides meaningful discussions on this issue; e.g., analysis and evaluation of the design factors and the appropriate control

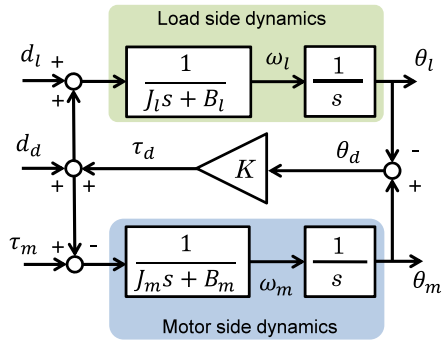

Fig. 2. Block diagram of the SEA modeled as a two-mass system.

variables in the DOB applied to an SEA. This analysis will enable a more effective application of the DOB to an SEA.

The main contribution of this paper are as follows:

1) the dynamic behavior of an SEA is modeled using the two-mass system;
2) model-based force control such as the DOB and feedforward control is designed to achieve high-precision SEA force control;
3) control performance and robustness are explored using theoretical analysis and experimental verification.

This paper is organized as follows. The dynamic model of the SEA is derived based on the two-mass model in Section II, including the effect of environments. The application of the DOB to SEA and its performance and robustness are addressed in Section III. The experiments utilizing an SEA system verifies the high performance of the proposed controller in Section IV. In Section V, conclusions are given.

II. Analysis of SEA Dynamics for Force Control

In this section, it is shown that an SEA can be modeled as a two-mass system, which has been utilized to model any flexible system in industrial applications. Contacts with environments can also be incorporated in this two-mass model.

A. Modeling of the SEA in Two-Mass System Representation (Without Contact With Environments)

Fig. 2 illustrates the dynamics of the SEA system as a two-mass system; it consists of motor side dynamics, a gear that amplifies the output force (torque) of the actuator, a spring placed between the load and the motor of an SEA, and load dynamics. The definitions of all the parameters in this paper are given in Table I.

Even though the load dynamics has not been included in many of conventional SEA models [10], [11], it can be incorporated in the model to describe the dynamic characteristics of the load part that is connected after the spring. The load dynamics may be complicated and nonlinear [15], but they can be represented by a simple inertia (J_l) and a damping coefficient (B_l) that may reflect the linear part of the complicated dynamics.

K is the spring constant that represents the elasticity of the spring. The variables θ_m and θ_l are the angular position measurements of the motor side and the load side, respectively, and θ_d is the difference between θ_m and θ_l ($\theta_d = N_m^{-1}\theta_m - \theta_l$),

TABLE I
NOMENCLATURE

J_m	Motor inertia	J_l	Load inertia
B_m	Motor damping	B_l	Load damping
K	Spring stiffness	N_m	Reduction ratio
C_{fb}	Feedback controller	C_{ff}	Feedforward controller
J_e	Inertia of environment	B_e	Damping of environment
K_e	Stiffness of environment	θ_m	Motor angle
θ_l	Load angle	θ_d	Spring deformation
ω_m	Motor velocity	ω_l	Load velocity
d_l	Disturbance on the load	d_d	Disturbance on the spring
θ_d^r	Desired spring deformation	τ_d^r	Desired spring force
$P_n(s)$	Nominal dynamic model	$Q(s)$	Q filter

i.e., the spring deflection. The two-mass system representing the SEA is subjected to various force inputs, such as a motor torque (i.e., τ_m), which is regarded as a control input to the SEA system, and a disturbance applied to the load (i.e., d_l) or to the spring (i.e., d_d).

The relationships among the inputs and outputs can be calculated as transfer functions based on the block diagram in Fig. 2, see (1) shown at the bottom of this page, which clarifies the dynamic relationships from force inputs and the position outputs. $P_m(s)$ describes the transfer function of the motor side dynamics, i.e., $P_m(s) = \frac{1}{s}\frac{1}{J_m s + B_m}$ in Fig. 2, and $P_l(s)$ describes the transfer function of the load-side dynamics that is $P_l(s) = \frac{1}{s}\frac{1}{J_l s + B_l}$. The common denominator $D(s)$ of the transfer functions is $D(s) = 1 + KN_m^{-2}(s)P_m(s) + KP_l(s)$.

The definition of *force control* is ambiguous [16] so that it covers from the precision control of the force output to the interaction control [4] and the impedance control [17]. In this paper, the force control aims to the control of the force transmitted to the load through the spring of an SEA, which corresponds to $\tau_d = K\theta_d$ in Fig. 2. The accuracy of the transmitted force with respect to the desired force is particularly the main concern in this paper.

For realizing the high-precision force control by an SEA, the spring deflection, θ_d, is selected as the control variable and is fed back to the system. Notice that the transmitted force τ_d is linearly proportional to θ_d, and thus, the force control problem can be converted into a position control problem. To generate the desired force, τ_d^r, the spring deflection is controlled to follow a reference trajectory, θ_d^r, which is calculated in real time as

$$\theta_d^r(t) = K^{-1}\tau_d^r(t). \tag{2}$$

In order to analyze and synthesize feedback controllers for the force control of an SEA, the open-loop dynamic model of the two-mass system is required, which is represented by the transfer function from the control inputs to the spring deflection. The transfer function is already derived in (1) and can be rewritten as

$$\Theta_d = \frac{N_m^{-1}P_m\mathcal{T}_m - P_l\mathcal{D}_l - (N_m^{-2}P_m + P_l)\mathcal{D}_d}{1 + KP_l + KN_m^{-2}P_m} \tag{3}$$

where $\Theta_d, \mathcal{T}_m$, and $\mathcal{D}_\bullet$ are the Laplace transforms of θ_d, τ_m, and $d_\bullet$, respectively. Notice that (3) is an open-loop nominal model, which is subjected to change due to the interaction with environment and the nonlinearity neglected in the linear model.

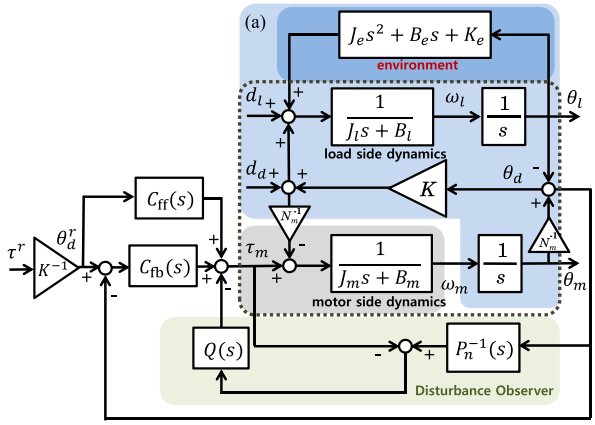

Fig. 3. Block diagram of the SEA and the environment with the proposed control algorithm.

B. Modeling of an SEA Contacting With Environments

When the SEA interacts with an environment the impedance of which is given as $J_e s + B_e + \frac{K_e}{s}$, it can be modeled and considered as in Fig. 3 (see the block labeled as "environment"). This configuration represents that the SEA is subjected to a double-layered interaction; the first layer is the inherent dynamics of the load side, $\frac{1}{s}\frac{1}{J_l s + B_l}$, and the second layer is the environment that has the impedance $J_e s + B_e + \frac{K_e}{s}$. Notice that contacting with environments can be considered the change of the load dynamics; the contact with the environment changes the load dynamics from $\frac{1}{s}\frac{1}{J_l s + B_l}$ to $\frac{1}{(J_l + J_e)s^2 + (B_l + B_e)s + K_e}$ equivalently.

When the load side of the SEA contacts a very stiff environment, the dynamics of the SEA is determined by limiting the environmental stiffness, K_e, to infinity, which results in $\theta_l = 0$. In this extreme case, the motor side of the SEA interacts with the environment through only its mechanical spring, and the overall

$$\begin{bmatrix} \theta_m \\ \theta_d \\ \theta_l \end{bmatrix} = \begin{bmatrix} \frac{P_m(1+KP_l)}{D(s)} & \frac{N_m^{-1}P_m}{D(s)} & \frac{KN_m^{-1}P_mP_l}{D(s)} \\ \frac{N_m^{-1}P_m}{D(s)} & \frac{-N_m^{-2}P_m - P_l}{D(s)} & -\frac{P_l}{D(s)} \\ \frac{KN_m^{-1}P_mP_l}{D(s)} & \frac{-P_l}{D(s)} & \frac{P_l(1+KN_m^{-2}P_m)}{D(s)} \end{bmatrix} \begin{bmatrix} \tau_m \\ d_d \\ d_l \end{bmatrix} \tag{1}$$

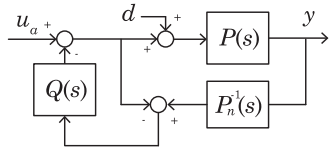

Fig. 4. Basic configuration of the DOB.

open-loop dynamics becomes

$$\Theta_d = \frac{N_m^{-1} P_m \mathcal{T}_m - N_m^{-2} P_m \mathcal{D}_d}{1 + K N_m^{-2} P_m}. \tag{4}$$

When the intrinsic disturbance d_d is zero, (4) is equivalent to the equation of motion, $N_m^2 (J_m \ddot{\theta}_d + B_m \dot{\theta}_d) + K\theta_d = N_m \tau_m$, which is a typical mass–spring–damper representation of the motor side dynamics.

III. Force Control of SEA Based on Dynamic Model

A. Introduction of a DOB

The design and analysis of force control systems contacting environments have been studied intensively in previous works. Many force control methodologies have been analyzed based on a simple proportional (P) control with appropriate stability conditions, such as passivity condition [4] or collocated system condition [5]. Taking these conditions into consideration, a phase lead compensator was proposed as a feedback controller to overcome the phase limitation and to obtain a higher frequency bandwidth than the typical P controller [18].

In these previous works, it has been commonly discussed that SEA has a limitation of bandwidth caused by its elasticity, and thus, an SEA has been considered inferior to rigid actuators when it comes to high power and high speed force generation. In this paper, the DOB and feedforward control based on it are employed to overcome this limitation and to achieve high-speed and high-precision force control of the SEA.

Fig. 4 is the basic configuration of the DOB, where $P_n(s)$ is the nominal transfer function of the SEA system from the motor torque (τ_m) to the spring deflection (θ_d), i.e.

$$P_n(s) = \frac{N_m^{-1} P_m}{1 + K P_l + K N_m^{-2} P_m}(s) \tag{5}$$

as in (1). $Q(s)$ is mostly designed as a low-pass filter that makes the DOB system robust and realizable. u_a is an auxiliary control input (which will be designed as $u_a = C_{\rm ff}(s)[\theta_d^r] + C_{\rm fb}(s)[\theta_d^r - \theta_d]$ later). d is a lumped disturbance including the model variation.

The closed-loop transfer functions of the DOB loop are

$$T_{u_a \to y}(s) = \frac{P}{1 - Q + QPP_n^{-1}}(s) \tag{6}$$

$$T_{d \to y}(s) = \frac{(1-Q)P}{1 - Q + QPP_n^{-1}}(s) \tag{7}$$

where $T_{\bullet \to \circ}$ represents the closed-loop transfer function from $\bullet$ to $\circ$. Note that the dynamic characteristic from u_a to y is nominalized to $P_n(s)$ by the DOB at frequencies where the Q filter is unity. Also the influence by the exogenous disturbance is fully rejected, i.e.

$$T_{u_a \to y}(s) \approx P_n \tag{8}$$

$$T_{d \to y}(s) \approx 0 \tag{9}$$

for $Q(s) = 1$. Such characteristics of the DOB are beneficial for the overall tracking control performance. Notice that as long as $Q(s) = 1$, the closed-loop dynamics is nominalized to P_n even in the presence of model variations, and the exogenous disturbance is effectively cancelled. This is why DOB is often considered a robust control algorithm.

DOBs have long been applied to industrial position control, and it is considered as an emerging control methodology for the SEA [19]–[21]. In comparison with these designs, this paper proposes a novel force control algorithm that includes the DOB and feedforward controller as in Fig. 3, which is an application of the two-degree-of-freedom (TDOF) control algorithm [22] to an SEA. The proposed controller has the following features, compared with the other conventional DOB applications.

1) The DOB is applied not to the motor angle but to the spring deflection so that it can normalize the dynamics of the spring deflection directly [23].
2) The DOB is designed in the most inner control loop so that the other outer control loop can benefit from the nominalization of the spring deflection dynamics by the DOB.
3) The feedforward controller is designed based on the nominalized model to improve the force control performance.

The feedforward control design in this paper is a unique point that distinguishes the proposed control algorithm from previous DOB applications to the SEA [19], [20]; the feedforward controllers in previous studies were based on mostly static characteristics of an SEA or designed very outside of the whole control configuration, while the proposed feedforward controller is based on the dynamic characteristic of the SEA exploiting the nominalization ability of DOB, and it is located in the most inner loop so as to achieve high-speed force control.

B. Improvement of Force Control Performance by DOB With Feedforward Control

Two-degree-of-freedom control for the SEA system consists of a feedback controller, $C_{\rm fb}(s)$, a feedforward controller, $C_{\rm ff}(s)$, and a DOB as illustrated in Fig. 3. The nominal plant model of the SEA system, $P_n(s)$ in (5), is utilized for the design of each controller in this paper; the DOB is designed based on the inverse plant model of the SEA, $P_n^{-1}(s)$, with a Q filter, $Q(s)$, and the feedforward controller is designed as the inverse plant model multiplied by a low-pass filter to make $C_{\rm ff}(s)$ proper. A proportional-integral-derivative (PID) controller is applied as $C_{\rm fb}(s)$, the gains of which can be tuned based on the nominal plant model.

Simulation study has been conducted with two different settings to verify the performance of the proposed controller design method; the first setting was to validate the improvement of tracking performance, and the second setting was to investigate the robustness of the proposed method against a modeling error. The dynamic model derived in (5) was utilized for the design

TABLE II
SIMULATION RESULTS: RMS ERRORS WITH VARIOUS REFERENCE SIGNALS

Controller type	0.5 Hz	1 Hz	5 Hz	Step
P	1.879e-1	1.740e-01	4.161e+00	5.008e-01
P with FF	6.797e-3	1.041e-02	8.962e-01	1.191e-01
P with FF and DOB	4.873e-3	9.071e-03	8.115e-01	8.305e-02
PI	6.823e-1	7.050e-01	7.159e-01	5.968e-01
PI with FF	2.265e-2	2.271e-02	1.537e-01	1.215e-01
PI with FF and DOB	1.401e-2	2.818e-02	1.407e-01	5.178e-02
PD	9.009e-3	7.975e-03	2.996e-02	1.006e-01
PD with FF	7.270e-4	1.458e-03	9.730e-03	9.733e-02
PD with FF and DOB	6.680e-4	1.324e-03	8.769e-03	9.146e-02
PID	4.104e-2	5.838e-02	2.334e-01	8.598e-02
PID with FF	9.233e-4	2.286e-03	5.119e-02	5.946e-02
PID with FF and DOB	1.061e-3	2.681e-03	4.649e-02	5.796e-02

of controllers, and the parameters for the model were obtained from an identification result given in Table III.

The first simulation setting was to assess the performance enhancement by the feedforward controller and the DOB. For this purpose, force tracking control was simulated with three different conditions: 1) $C_{\rm fb}$ only, 2) $C_{\rm fb}$ and $C_{\rm ff}$, and 3) $C_{\rm fb}$, $C_{\rm ff}$, and the DOB. The root mean square (RMS) errors were measured and compared with these three cases. In addition, four different types of PID controllers (i.e., P, PI, PD, and PID) were applied as $C_{\rm fb}$, and the control parameters were tuned using the `pidtune` command in MATLAB with the nominal plant dynamics, $P_n(s)$.

In order to assess the control performance, four different force reference trajectories, which include sinusoidal waveforms of 0.5, 1, and 5 Hz and a rectangular waveform, were applied. The Q filter in the DOB is a first-order low-pass filter with the cutoff frequency of 50 Hz, and a second-order low-pass filter with the same cutoff frequency was applied to $C_{\rm ff}$ for realizability.

For realistic simulations under a practical setting, the backlash of 1 degree was applied between the gears, and the quantization effect, which corresponds to the actual encoders used in experiments, was applied to θ_l and θ_m. All the controllers, $C_{\rm ff}$, $C_{\rm fb}$, and DOB, were implemented with the sampling period of 1 ms.

Table II shows the result of the force reference tracking control simulations; the RMS values of the tracking errors are compared in the table. It can be observed through this simulation study that:

1) the proposed control algorithm including the DOB and feedforward controller can improve the force tracking performance;
2) the DOB and feedforward controller can improve the performance of feedback controllers, regardless of their types (i.e., P, I, D, or any of their combinations).

In this simulation, the same model was applied to both the controller design and the simulation of the plant dynamics. The dynamic characteristics of an SEA system in practice, however, may not be identified accurately and may frequently change over time, which may deteriorate the control performance by the feedback and feedforward control. In this aspect, the DOB is very effective, since it rejects the modeling error, as well as an exogenous disturbance, such that the plant dynamics follows the nominal model.

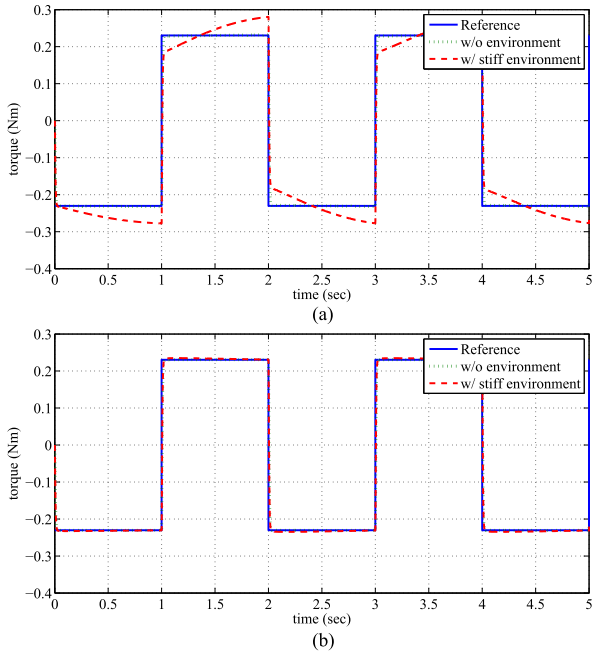

Fig. 5. Force tracking performance with feedfoward control.

In order to validate this robustness by the DOB, simulations with large modeling error were carried out with two different controller configurations: one with $C_{\rm fb}(s) = k_P$ and $Q(s) = 0$ (which means without DOB), and the other one with the same $C_{\rm fb}(s)$ and DOB with $Q(s) = (\frac{20\pi}{s+20\pi})$, i.e., a low-pass filter with the cut-off frequency of 10 Hz. In both cases, $C_{\rm ff}(s)$ was designed as the inverse of the nominal model given in (5) followed by a second-order low-pass filter with the cutoff frequency of 50 Hz. The k_P gain was designed for the nominal model in (3) to obtain 60° of phase margin by the command `pidtune`. For each simulation setting, the contribution of the DOB to the feedforward control was examined by changing the environment condition. Two situations were assumed: a fully constrained case and a free case. In the free case, $J_e = 0$, $B_e = 0$, and $K_e = 0$. On the other hand, in the fully constrained case, the environmental parameters were set to $J_l = 0$, $B_e = 5B_l$, and $K_e = 200K$ to simulate a stiff environment. This change of the environmental parameters would introduce a meaningful model variation into the SEA control system.

Fig. 5 shows the simulation results, where Fig. 5(a) is the result without the DOB, and Fig. 5(b) is the result with the DOB. In both figures, the dotted lines are the results in the nonconstrained situation and the dashed lines are ones in the constrained situation. Without the environmental constraint, which was the nominal model case, the control system could achieve good force tracking performances regardless of the DOB. When the SEA contacted the stiff environment, however, the model changed much, and the effectiveness of the DOB was clearly shown; notice that the force control performance was maintained almost same even with the model variation. This is due to the nominalization ability of the DOB; even when the load-side dynamics changes by the environmental conditions, DOB compensates for the change, and the overall control performance can be maintained even in the presence of the modeling error, as well as disturbances.

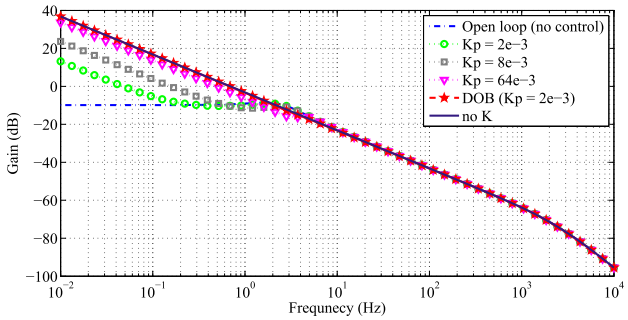

Fig. 6. Frequency response from d_d to θ_L.

C. High-Bandwidth Compliance Achieved by the DOB

In addition to the force tracking performance, force regulation or disturbance rejection performance is another important requirement of the force control. It should be noted that the disturbance rejection of the force control system works differently from that of position control; the reaction force by the position control to reject the disturbance should be large enough to keep the desired position, while the reaction force by the force control to reject the disturbance should be as much as the desired interaction force: it should be as small as possible when the desired interactive force is set to 0.

The ZIC is a force controller that is requested to generate no resistance to the load-side movement. The ZIC can be carried out by setting $\theta_d = 0$; namely, the force controller controls the spring deflection (i.e., the transmitted force) to be zero no matter what happens on the load side.

The dynamic characteristics of the spring deformation can be utilized to explore how the DOB can improve the performance of ZIC in practice. The dynamics of the spring deflection under a proportional feedback controller, $\tau_m = C_{\rm fb}[\theta_d^r - \theta_d]$ without the DOB (i.e., $Q(s) = 0$) can be obtained from Fig. 3, i.e.,

$$\Theta_d = \frac{N_m^{-1}P_m C_{\rm fb}\Theta_d^r - P_l\mathcal{D}_l - (N_m^{-2}P_m + P_l)\mathcal{D}_d}{1 + KP_l + KN_m^{-2}P_m + N_m^{-1}P_m C_{\rm fb}} \quad (10)$$

where θ_d^r is the reference signal for θ_d calculated as in (2), and Θ_d^r is its Laplace transform. Also the spring deflection dynamics with DOB is given as

$$\Theta_d = \frac{N_m^{-1}P_m C_{\rm fb}\Theta_d^r - (1-Q)\left[P_l\mathcal{D}_l + (N_m^{-2}P_m + P_l)\mathcal{D}_d\right]}{1 + KP_l + KN_m^{-2}P_m + N_m^{-1}P_m C_{\rm fb}}. \quad (11)$$

Notice that DOB does not influence the dynamic characteristic from the reference θ_d^r to the spring deflection, while it has a large effect on the dynamics against the exogenous forces d_d and d_l; $(1-Q)$ is multiplied to the transfer functions with regard to the exogenous force inputs. It can be easily concluded that the effect of the exogenous forces on the output force will be eliminated when $Q(s)$ is unity, which means that the zero impedance can ideally be realized at frequencies where the $Q(s) \approx 1$ leaving no reaction force from the spring against the external forces.

Fig. 6 shows the frequency characteristics from d_d to θ_l with various control conditions, which were obtained based on the parameters in Table III. Notice that the dashed line labeled as "no K" represents the dynamic characteristic of the load side when it is disconnected from the elasticity, i.e., $\frac{1}{J_l s^2 + B_l s}$. It can be observed that a higher feedback control gain could achieve disconnection from the elasticity making the frequency response converge to that of $\frac{1}{J_l s^2 + B_l s}$. On the other hand, with DOB, the frequency response is almost the same as that of $\frac{1}{J_l s^2 + B_l s}$ even with the low feedback control gain, which shows that the proposed DOB can achieve better ZIC performance without increasing the gain.

D. Difference From Conventional DOB Application to the Two-Mass System

Application of DOBs to two-mass systems can be found in literature [12], [13], [24]. Most articles, however, applied the DOB design methodology to the motor-side angle θ_m, instead of θ_d. This difference is due to the difference of purposes; the conventional DOB for two-mass systems is to achieve high-performance position control of θ_m and θ_l, while the proposed DOB is to achieve high-precision force control. In other words, the DOB on θ_m produces high reactive force against external forces, while the DOB on θ_d produces little reactive force.

Nevertheless, the conventional DOB with θ_m can be utilized for force control as in [15]; at first, a high-performance tracking controller for θ_m is designed using the conventional DOB, and the position reference θ_m^r is designed with regard to the desired spring deflection and the load-side motion θ_l, i.e., $\theta_m^r = N_m(K^{-1}\tau^r + \theta_l)$, such that the force reference τ^r can be realized by precisely tracking the motor reference.

However, the performance by this conventional motor-position-based DOB approach is different from the proposed DOB, which can be analyzed by comparison of transfer functions. Equation (12) is the transfer function from the torque reference τ^r and the exogenous force inputs d_d and d_l to the spring deformation θ_d under the conventional DOB using θ_m and a feedback controller $C_{\rm fb}(s)$

$$\begin{aligned}\Theta_d = {} & \frac{N_m^{-1}P_m C_{\rm fb}}{1 + KP_l + KN_m^{-2}P_m + N_m^{-1}P_m C_{\rm fb}}\Theta_d^r \\ & - \frac{P_l(1 + KP_l + KN_m^{-2}P_m Q)}{(1+KP_l)(1+KP_l+KN_m^{-2}P_m + N_m^{-1}P_m C_{\rm fb})}\mathcal{D}_l \\ & - \frac{(1-Q)N_m^{-2}P_m + P_l(1 + KP_l + KN_m^{-2}P_m)}{(1+KP_l)(1+KP_l+KN_m^{-2}P_m + N_m^{-1}P_m C_{\rm fb})}\mathcal{D}_d. \end{aligned} \quad (12)$$

Compared to the transfer function in (11), i.e., the closed-loop dynamics with the proposed control scheme in this paper, the response to the reference θ_d^r is the same. It should be noted that the dynamics from d_l and d_d, however, are much different; in particular, when $Q(s) \sim 1$, the transfer functions from d_d and d_l in (12) are approximated to

$$-\frac{P_l}{1 + KP_l} \quad (13)$$

while it is fully eliminated by the proposed structure as in (11).

This shows that the dynamics of the load side under the conventional DOB is decoupled from the motor dynamics, i.e., $\frac{1}{J_m s^2 + B_m s}$, while it is still coupled with the spring elasticity K. Consequently, it can be concluded that the force control based on the conventional DOB has inferior performance to the proposed force control when it comes to ZIC; the interactive force will be affected by the elasticity of SEA. On the other hand, the proposed DOB can decouple the effect of the spring elasticity, leaving the impedance of the load side only, i.e., $P_l = \frac{1}{J_l s^2 + B_l s}$ which is disconnected and free from the elasticity and demonstrating better ZIC performance.

E. Robust Stability Against Changes of Environmental Parameters

As explained in Section II-B, the load-side dynamics can vary depending on the environment with which the load-side interacts. This causes parameter variations from the nominal model utilized in the DOB design. The stability of the system with the proposed DOB under the modeling error can be evaluated using the small gain theorem [25] as

$$|Q(j\omega)W(j\omega)| < 1 \text{ for all } \omega \in \mathbb{R} \tag{14}$$

where $W(j\omega)$ describes the envelop curve of all possible modeling errors in a multiplicative model uncertainty representation, i.e., $P(s) \in \{P_n(s)(1 + W(s)\Delta(s)) : W(s) \in \mathcal{R}, \|\Delta\|_\infty < 1\}$ as

$$|W(j\omega)| > \left| \frac{P(j\omega) - P_n(j\omega)}{P_n(j\omega)} \right| \tag{15}$$

for all ω and actual plants $P(j\omega)$.

When the SEA contacts a stiff environment, the environmental stiffness becomes infinite, and thus, the magnitude of multiplicative uncertainty becomes maximal. In this case, the transfer function becomes (4), and the modeling error envelop curve for this case, $W_{\text{con}}(s)$, is determined by assuming $\Delta(s) = 1$ as

$$W_{\text{con}}(s) = \frac{P_{\text{con}}(s) - P_n(s)}{P_n(s)} \tag{16}$$

where the nominal plant is $P_n(s) = \frac{N_m^{-1} P_m}{1 + K P_l + K N_m^{-2} P_m}$ and the dynamics of the plant under the contact with stiff environments, P_{con}, is given as

$$P_{\text{con}}(s) = \frac{N_m^{-1} P_m}{1 + K N_m^{-2} P_m} \tag{17}$$

as derived in Section II-B.

Assuming that the stiff environment condition imposes the maximal model variation, the robust stability can be evaluated by checking if

$$|Q(j\omega)| < |W_{\text{con}}^{-1}(j\omega)| \tag{18}$$

for all $\omega \in \mathbb{R}$. In order to investigate the robust stability using (18), the modeling uncertainties defined in (15) should be calculated for all possible conditions on the environment. Notice that changing J_l and B_l is equivalent to changing J_e and B_e of the environments, and this model uncertainty is considered to have an upper limit, which is the case when the environment has infinity impedance. Fig. 7 shows $W^{-1}(s)$'s when J_l and B_l increase, and finally, converge to the case where the environment has infinity impedance ($J_l \to \infty$ and $B_l \to \infty$).

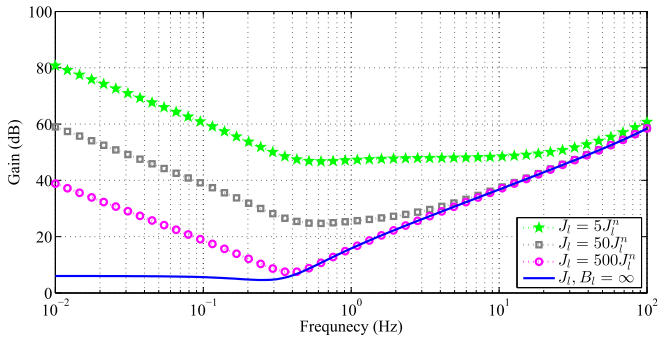

Fig. 7. Robustness against the variation of inertia J_l.

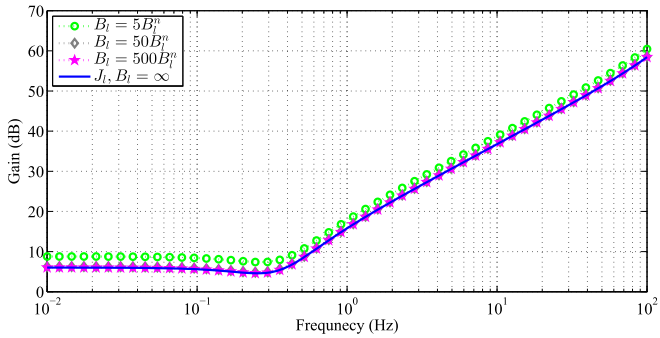

Fig. 8. Robustness against the variation of damping B_l.

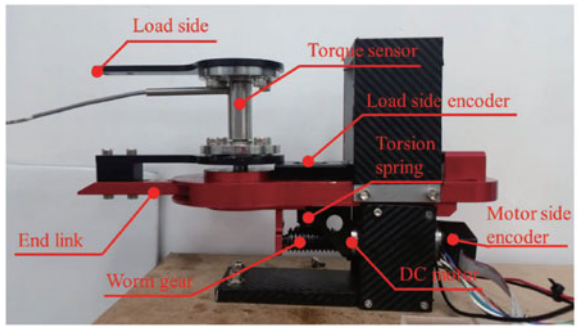

Fig. 9. Experimental setup of an SEA.

It should be noted that the gain characteristics of $W^{-1}(j\omega)$ in Figs. 7 and 8 are above 0 dB. This implies that the Q filter, which is designed as a low-pass filter, does not cross over the magnitude of $W^{-1}(j\omega)$, and therefore, the robust stability is guaranteed against these parameter variations based on (18).

IV. Experimental Results

A. Experimental Setup and Parameter Identification

In order to verify the performances of the proposed SEA force control method, an experimental setup shown in Fig. 9, a compact rotary SEA (cRSEA) system, is utilized. The detailed mechanical design of the cRSEA can be found in [26]. It consists of

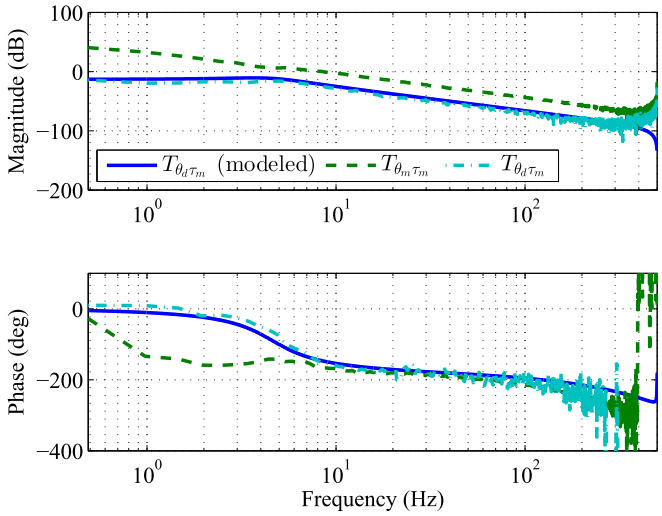

Fig. 10. Frequency responses of cRSEA from the motor torque input to the three position measurements.

TABLE III
IDENTIFIED PARAMETERS

J_m	5.2500e−6 kg·m^2	J_l	0.0225 kg·m^2
B_m	4.5356e−6 Nm·s/rad	B_l	0.4697 Nm·s/rad
K	0.48 Nm/rad	N_m	20

a brushed dc motor (RE40 manufactured by Maxon Motor Co.) that has the power of 150 W. The motor is equipped with a set of gears, and the overall gear ratio is about 20:1. At both the motor side and load side, two encoders are installed to measure the angular positions of the two sides separately. For more objective comparison of the force control performance, a torque sensor is additionally utilized at the load side, as shown in the figure. The torque sensor is to measure the interaction torque between the load and the environment, while the spring deflection (i.e., the difference between the two encoder measurements) is to measure the torque transmitted through the spring. Therefore, the torque sensor enables checking of how controllers successfully control the device including the load-side dynamics.

In order to identify the parameters of the cRSEA, frequency responses were first obtained using an fast-Fourier-transform (FFT) analyzer (CF-9400 model manufactured by ONO-Sokki), as shown in Fig. 10. Frequency responses in the figure indicate the measured frequency responses from the motor torque input (τ_m) to two measurements (θ_m and θ_d), which are denoted by $T_{\theta_m \tau_m}$ and $T_{\theta_d \tau_m}$, respectively, in the figure. Based on the measured frequency responses, the parameters of the overall system dynamics, shown in Fig. 2, were identified to fit the frequency response curve. The solid line in Fig. 10 is the fitted frequency response calculated using the identified parameters in Table III.

B. Force Tracking Control Experiments

At first, the performance of the proposed SEA force control is evaluated by force tracking control experiments with three different controller settings: 1) $C_{\rm fb}(s) = k_P$, $C_{\rm ff}(s) = 0$, and $Q(s) = 0$; 2) $C_{\rm fb}(s) = k_P$, $C_{\rm ff}(s) = (\frac{100\pi}{s+100\pi})^2 P_n^{-1}(s)$, and $Q(s) = 0$; and 3) $C_{\rm fb}(s) = k_P$, $C_{\rm ff}(s) = (\frac{100\pi}{s+100\pi})^2 P_n^{-1}(s)$, and $Q(s) = \frac{20\pi}{s+20\pi}$, which were the same settings as the simulation study in Section III-B. k_p was set to 0.065, which is the tuned value using `pidtune` in MATLAB. The identified parameters in Table III are utilized in $P_n^{-1}(s)$ design. It should be noted that $P_n(s)$ utilized for the DOB design is the dynamic model of the SEA without contacting with environments, which is given as (3). In the following experiments, however, the load side of the SEA is constrained by a stiff environment, and thus, there is a large model discrepancy from this nominal model.

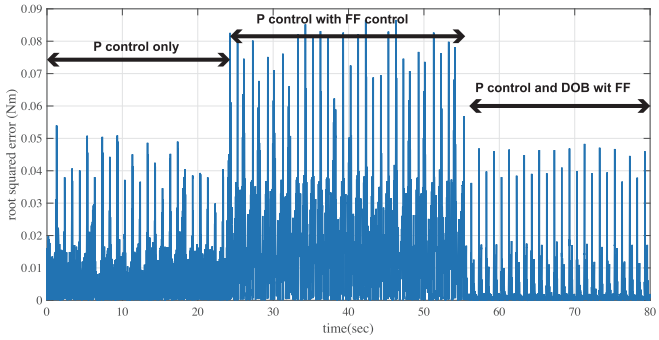

Fig. 11. RS values of force tracking error for a 0.5-Hz sinusoidal reference.

TABLE IV
RS VALUES OF FORCE TRACKING ERRORS FOR DIFFERENT FREQUENCY REFERENCES

Frequency	P only	P with FF	DOB with FF
0.1 Hz	0.02122	0.02221	0.003536
0.5 Hz	0.01257	0.02224	0.006533
1 Hz	0.02848	0.06598	0.01397
5 Hz	0.08412	0.1395	0.02496
10 Hz	0.3879	0.3978	0.09908

Fig. 11 shows the force tracking errors by the three controller settings for a sinusoidal torque reference, the frequency and the amplitude of which were set to 0.5 Hz and 0.3 Nm, respectively. The force control settings were switched from 1) to 2) at 24 s, and from 2) to 3) at 55.5 s. The figure shows the root squared (RS) force tracking error values (i.e., $K\sqrt{(\theta_d^r - \theta_d)^2}$) during the experiments.

The experimental results in Fig. 11 verified that the force tracking error is decreased by the DOB and feedforward control. The same experiments were carried out for the other references with different frequencies: 0.1, 1, 5, and 10 Hz. The RMS values of errors were calculated as in Table IV. Notice that the DOB successfully compensated for the model discrepancy, such that it can keep the frequency bandwidth of the model-based feedforward control up to the high frequency range.

C. ZIC Experiments

In order to evaluate the performance of the proposed controller as ZIC applications, forced movements were imposed on the load side by a human with certain patterns, as shown in Fig. 12(a), and the resultant resistive torque generated from

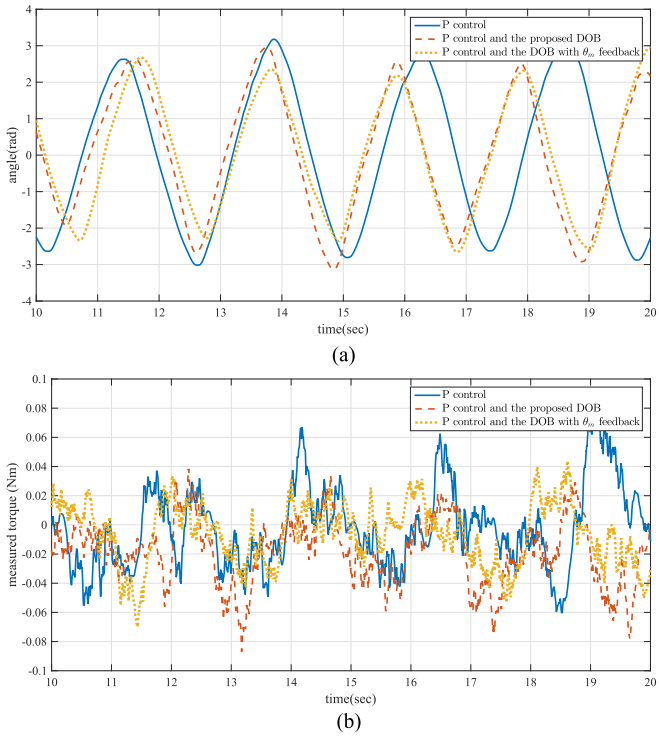

Fig. 12. Frequency responses of the dynamic models.

TABLE V
RMS VALUES OF MEASURED TORQUE

Frequency	P only	DOB with θ_m	DOB with θ_d
0.5 Hz	0.05246	0.04677	0.040767
1 Hz	0.09083	0.06510	0.06111
2 Hz	0.2131	0.1492	0.09377
4 Hz	1.776	0.9787	0.2968

the SEA was measured by an additional torque sensor (see the experimental setup in Fig. 9).

Three different force controller settings were implemented for the experiments to verify the discussion in Section III-C: 1) $C_{\rm fb}(s) = k_P$ without DOB; 2) $C_{\rm fb}(s) = k_P$ and the conventional DOB with θ_m feedback; and 3) $C_{\rm fb}(s) = k_P$ and the proposed DOB with θ_d feedback.

The impedance of the cRSEA is evaluated using four different movements with different periods, 0.5, 1, 2, and 4 Hz imposed on the load side, and the generated resistive torques were measured. The ratios of the magnitudes of resistive torques with respect to the load-side movements are calculated to indicate the impedance of the cRSEA. Throughout these experiments, the desired torque was set to zero so that the ZIC performance can be tested.

The experimental results are shown in Fig. 12(b), which verifies that the impedance was most reduced with the proposed DOB. For the quantitative comparison, Table V shows the ratio of the RMS values of the measured resistive torques with regard to the RMS values of the load-side displacements. The result shows that the impedance can be reduced up to the high frequency range with the proposed DOB, while the other conventional controllers (including a conventional DOB) cannot achieve the same performance. This verifies that the proposed control system shows a good disturbance rejection function with a large frequency range.

V. CONCLUSION

SEAs have been considered to have limitations due to dynamic characteristic, which is mostly attributed to the elasticity in the SEA. This paper proposed that this limitation can be overcome when the controller is designed taking account of the dynamic characteristics of the SEA.

First, it was shown in this paper that the SEA can be modeled as the two-mass system, which also can include the environmental impedance. Then, DOB and the feedforward control were designed in the proposed controller fully utilizing the dynamic model, and its superior performance has been confirmed through experiments. Force tracking performance and zero-impedance performance with regard to the external force were verified through experiments, and the robustness of the proposed control and its advantage over the conventional DOB application to the SEA have been shown.

Based on the derived dynamic models and the experiments of the proposed force control, it was found in this paper that: 1) the high-performance force control of the SEA can be achieved utilizing the dynamic characteristic of the spring deflection and controlling it; 2) a feedforward controller is necessary for obtaining the desired force control performance; and 3) DOB can be successfully applied to the control of the spring deflection, nominalizing the dynamic characteristic of it.

REFERENCES

[1] S. Haddadin, A. Albu-Schaffer, and G. Hirzinger, "The role of the robot mass and velocity in physical human-robot interaction—Part I: Non-constrained blunt impacts," in *Proc. IEEE Int. Conf. Robot. Autom.*, May 2008, pp. 1331–1338.

[2] S. Oh *et al.*, "A generalized control framework of assistive controllers and its application to lower limb exoskeletons," *Robot. Auton. Syst.*, vol. 73, pp. 68–77, 2015. [Online]. Available: http://www.sciencedirect.com/science/article/pii/S092188901400219X

[3] W. S. Newman, "Stability and performance limits of interaction controllers," *J. Dyn. Syst., Meas. Control*, vol. 114, no. 4, pp. 563–570, 1992, doi: 10.1115/1.2897725. [Online]. Available: http://dx.doi.org/10.1115/1.2897725

[4] E. Colgate and N. Hogan, "An analysis of contact instability in terms of passive physical equivalents," in *Proc. IEEE Int. Conf. Robot. Autom.*, vol. 1, May 1989, pp. 404–409.

[5] S. Eppinger and W. Seering, "Three dynamic problems in robot force control," *IEEE Trans. Robot. Autom.*, vol. 8, no. 6, pp. 751–758, Dec. 1992.

[6] S. Buerger and N. Hogan, "Complementary stability and loop shaping for improved human–robot interaction," *IEEE Trans. Robot.*, vol. 23, no. 2, pp. 232–244, Apr. 2007.

[7] A. Calanca, L. Capisani, and P. Fiorini, "Robust force control of series elastic actuators," *Actuators*, vol. 3, no. 3, pp. 182–204, 2014.

[8] D. E. Whitney, "Force feedback control of manipulator fine motions," *J. Dyn. Syst., Meas. Control*, vol. 99, no. 2, pp. 91–97, 1977, doi: 10.1115/1.3427095. [Online]. Available: http://dx.doi.org/10.1115/1.3427095

[9] G. Pratt and M. Williamson, "Series elastic actuators," in *Proc. IEEE/RSJ Int. Conf. Intell. Robots Syst.*, vol. 1, Aug. 1995, pp. 399–406.

[10] N. L. Tagliamonte and D. Accoto, "Passivity constraints for the impedance control of series elastic actuators," *Proc. Inst. Mech. Eng., I, J. Syst. Control Eng.*, vol. 228, no. 3, pp. 138–153, 2014. [Online]. Available: http://pii.sagepub.com/content/228/3/138.abstract

[11] H. Vallery *et al.*, "Compliant actuation of rehabilitation robots," *IEEE Robot. Autom. Mag.*, vol. 15, no. 3, pp. 60–69, Sep. 2008.

[12] Y. Hori, "A review of torsional vibration control methods and a proposal of disturbance observer-based new techniques," in *Proc. 13th IFAC World Congr.*, 1996.
[13] J. N. Yun, J. Su, Y. I. Kim, and Y. C. Kim, "Robust disturbance observer for two-inertia system," *IEEE Trans. Ind. Electron.*, vol. 60, no. 7, pp. 2700–2710, Jul. 2013.
[14] T. Boaventura *et al.*, "On the role of load motion compensation in high-performance force control," in *Proc. 2012 IEEE/RSJ Int. Conf. Intell. Robots Syst.*, Oct. 2012, pp. 4066–4071.
[15] K. Kong, J. Bae, and M. Tomizuka, "Control of rotary series elastic actuator for ideal force-mode actuation in human-robot interaction applications," *IEEE/ASME Trans. Mechatronics*, vol. 14, no. 1, pp. 105–118, Feb. 2009.
[16] A. Calanca, R. Muradore, and P. Fiorini, "A review of algorithms for compliant control of stiff and fixed-compliance robots," *IEEE/ASME Trans. Mechatronics*, vol. 21, no. 2, pp. 613–624, Apr. 2016.
[17] N. Hogan, "Impedance control: An approach to manipulation: Part I—Theory," *J. Dyn. Syst., Meas. Control*, vol. 107, no. 1, pp. 1–7, 1985, 10.1115/1.3140702. [Online]. Available: http://dx.doi.org/10.1115/1.3140702
[18] S. Eppinger and W. Seering, "On dynamic models of robot force control," in *Proc. 1986 IEEE Int. Conf. Robot. Autom.*, vol. 3, Apr. 1986, pp. 29–34.
[19] N. Paine, S. Oh, and L. Sentis, "Design and control considerations for high-performance series elastic actuators," *IEEE/ASME Trans. Mechatronics*, vol. 19, no. 3, pp. 1080–1091, Jun. 2014.
[20] J. S. Mehling, J. Holley, and M. K. O'Malley, "Leveraging disturbance observer based torque control for improved impedance rendering with series elastic actuators," in *Proc. 2015 IEEE/RSJ Int. Conf. Intell. Robots Syst.*, Sep. 2015, pp. 1646–1651.
[21] E. Sariyildiz, G. Chen, and H. Yu, "Robust position control of a novel series elastic actuator via disturbance observer," in *Proc. 2015 IEEE/RSJ Int. Conf. Intell. Robots Syst.*, Sep. 2015, pp. 5423–5428.
[22] T. Umeno, T. Kaneko, and Y. Hori, "Robust servosystem design with two degrees of freedom and its application to novel motion control of robot manipulators," *IEEE Trans. Ind. Electron.*, vol. 40, no. 5, pp. 473–485, Oct. 1993.
[23] S. Oh, C. Lee, and K. Kyoungchul, "Force control and force observer design of series elastic actuator based on its dynamic characteristics," in *Proc. 41th Annu. Conf. IEEE Ind. Electron. Soc.*, Nov. 2015, pp. 4639–4644.
[24] S. Katsura and K. Ohnishi, "Force servoing by flexible manipulator based on resonance ratio control," *IEEE Trans. Ind. Electron.*, vol. 54, no. 1, pp. 539–547, Feb. 2007.
[25] C. Kempf and S. Kobayashi, "Disturbance observer and feedforward design for a high-speed direct-drive positioning table," *IEEE Trans. Control Syst. Technol.*, vol. 7, no. 5, pp. 513–526, Sep. 1999.
[26] K. Kong, J. Bae, and M. Tomizuka, "A compact rotary series elastic actuator for human assistive systems," *IEEE/ASME Trans. Mechatronics*, vol. 17, no. 2, pp. 288–297, Apr. 2012.

Sehoon Oh (S'05–M'06) received the B.S., M.S., and Ph.D. degrees in electrical engineering from the University of Tokyo, Tokyo, Japan, in 1998, 2000, and 2005, respectively.

He worked as an Assistant Professor with the University of Tokyo until 2012 and was a Visiting Researcher with the University of Texas at Austin from 2010 to 2011. After working as a Senior Research with Samsung Heavy Industries and as a Research Professor at the Department of Mechanical Engineering, Sogang University, he is currently an Assistant Professor with Daegu Gyeongbuk Institute of Science and Technology, Daegu, South Korea. His research interests include the development of human-friendly motion control algorithms and assistive devices for people.

Dr. Oh received the Best Transactions Paper Award from the IEEE TRANSACTIONS ON INDUSTRIAL ELECTRONICS in 2013.

Kyoungchul Kong (S'04–M'09) received the B.Eng. degree in mechanical engineering, (*summa cum laude*) in 2004, the B.S. degree in physics in 2004, and the M.S. degree in mechanical engineering in 2006, all from Sogang University, Seoul, Korea, and the Ph.D. degree in mechanical engineering from the University of California, Berkeley, in 2009.

In 2011, he joined the Department of Mechanical Engineering, Sogang University. He has authored or coauthored more than 100 technical articles in journals and conference proceedings in the area of mechatronics, including locomotive robotics and human robot interactive systems. His current research interests include design, modeling, and control of mechatronic systems with emphasis on locomotion and mobility of robotic systems.

Dr. Kong received the Young Researcher Award of the International Federation of Automatic Control Mechatronics Technical Committee in 2016, the Best Student Paper Award at the IEEE Conference on Advanced Intelligent Mechatronics in 2008, and the Best Paper Award in the Division of Dynamic Systems and Control at the Korean Society of Mechanical Engineers Annual Conference in 2005.